Electronic Supplementary Information

A blessing and a curse: impact of urea derivatives on the secondary building unit of Ca-MOFs prepared in deep eutectic solvents

Michael Teixeira,[a] Benoît Louis[b] and Stéphane A. Baudron*[a]

a. Université de Strasbourg, CNRS, CMC UMR 7140, 4 rue Blaise Pascal, F-67000 Strasbourg, France. E-mail : sbaudron@unistra.fr

b. Université de Strasbourg, CNRS, ICPEES UMR 7515, 25 rue Becquerel, F-67087 Strasbourg, France.

X-ray powder diffraction

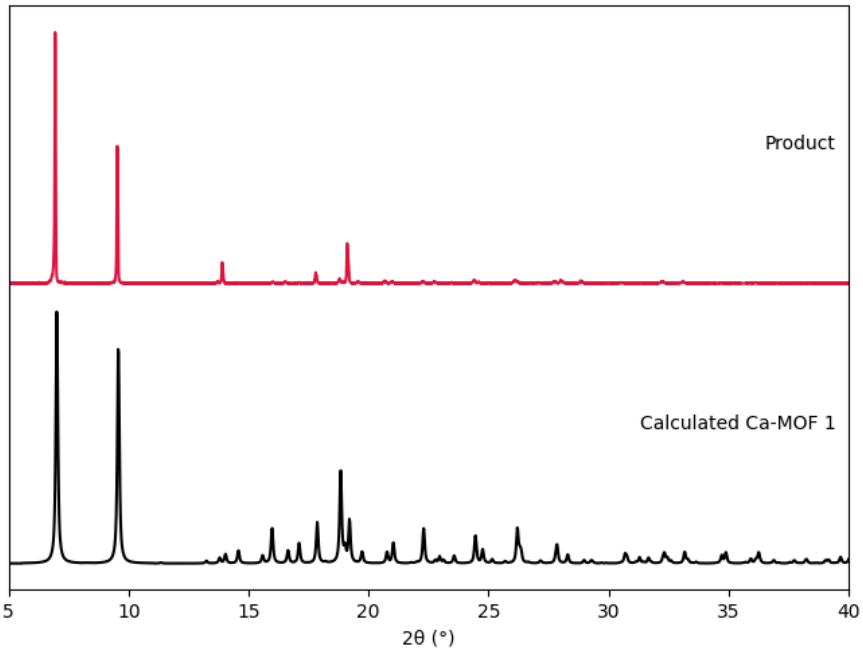

Fig. ESI1. Comparison of the PXRD diffractogram of a batch of Ca-MOF **1** (red, top) with the diagram calculated from single-crystal data (black, bottom).

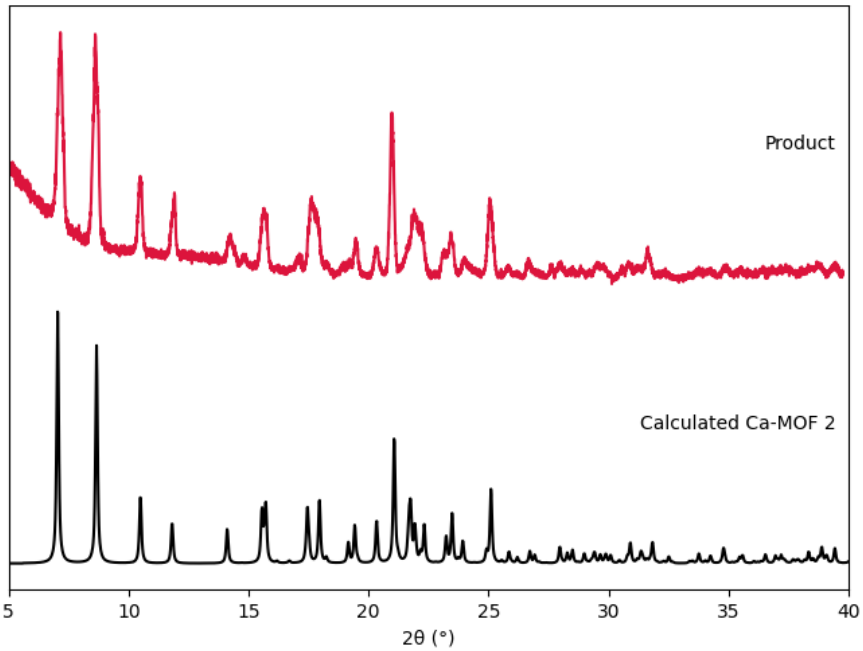

Fig. ESI2. Comparison of the PXRD diffractogram of a batch of Ca-MOF **2** (red, top) with the diagram calculated from single-crystal data (black, bottom). Broadening of the peaks is due to sensitivity to ambient conditions (humidity).

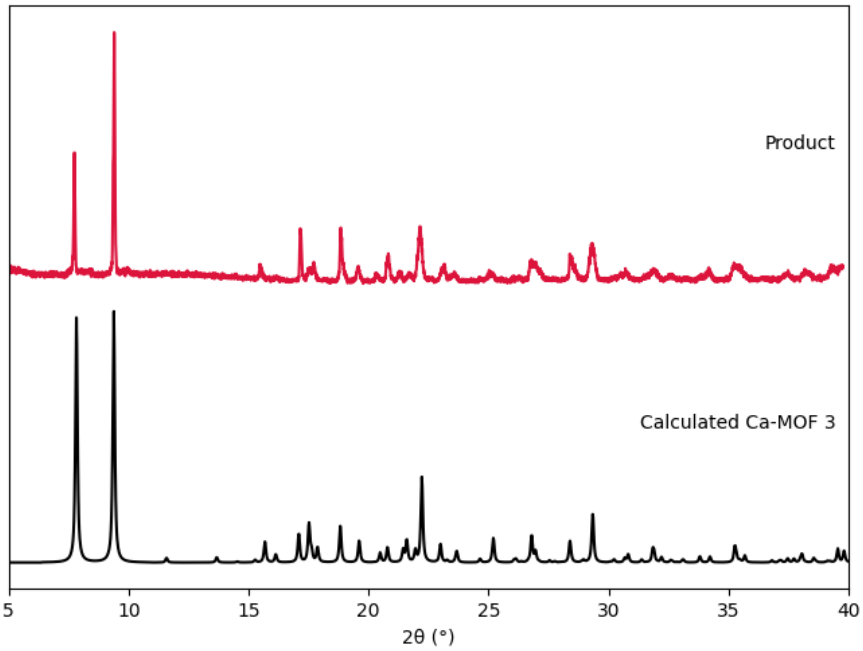

Fig. ESI3. Comparison of the PXRD diffractogram of a batch of Ca-MOF **3** (red, top) with the diagram calculated from single-crystal data (black, bottom).

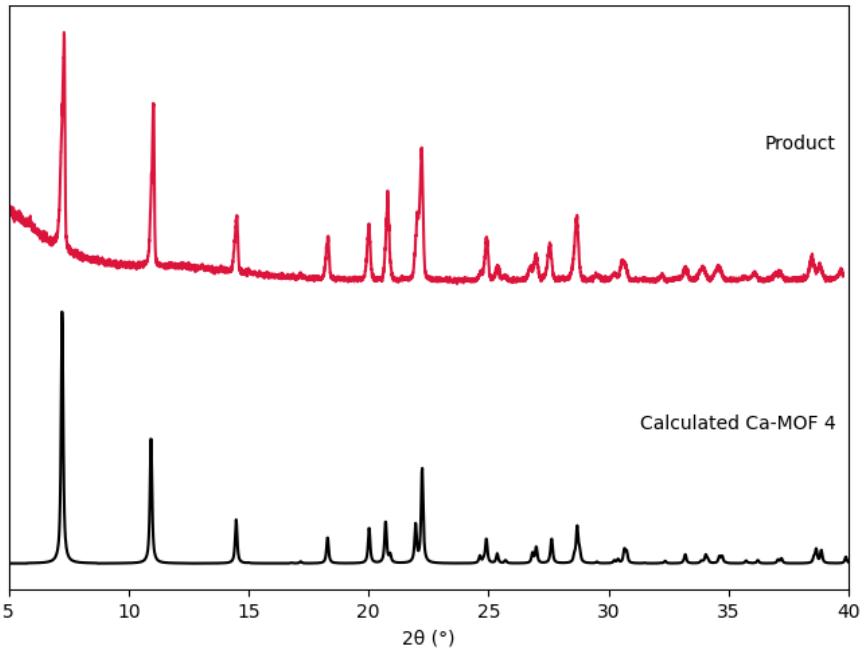

Fig. ESI4. Comparison of the PXRD diffractogram of a batch of Ca-MOF **4** (red, top) with the diagram calculated from single-crystal data (black, bottom).

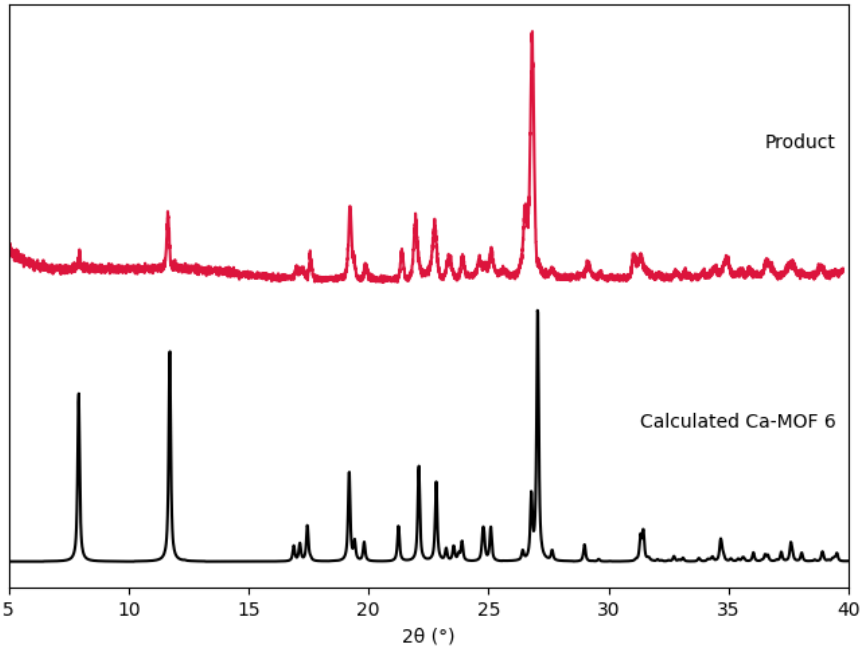

Fig. ESI5. Comparison of the PXRD diffractogram of a batch of Ca-MOF **6** (red, top) with the diagram calculated from single-crystal data (black, bottom).

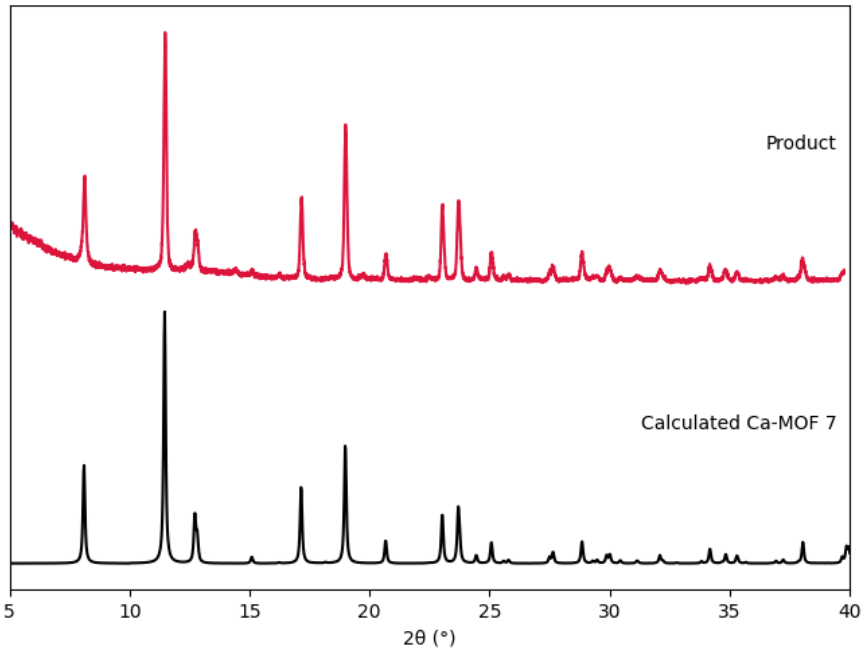

Fig. ESI6. Comparison of the PXRD diffractogram of a batch of Ca-MOF **7** (red, top) with the diagram calculated from single-crystal data (black, bottom).

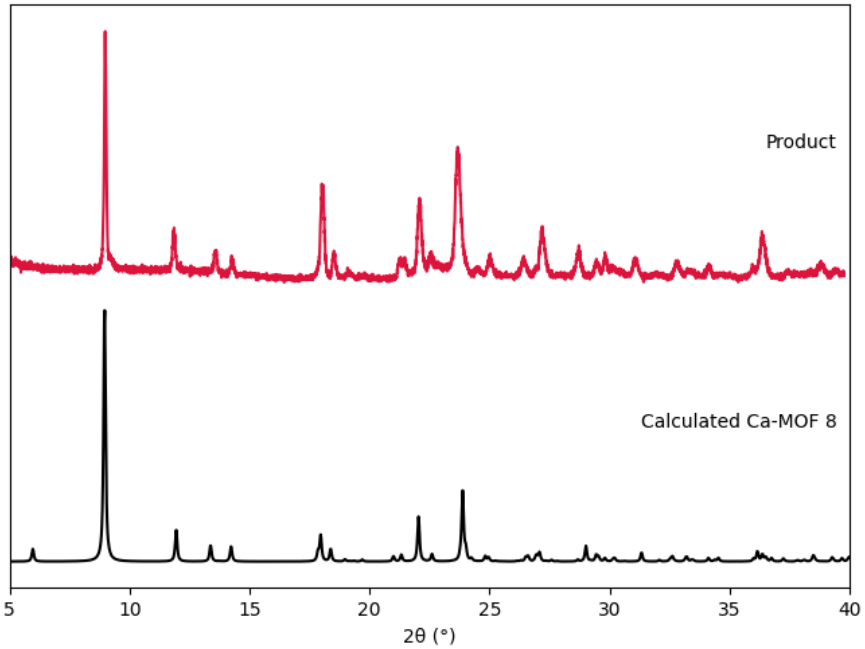

Fig. ESI7. Comparison of the PXRD diffractogram of a batch of Ca-MOF **8** (red, top) with the diagram calculated from single-crystal data (black, bottom). The peak at 5.95° is missing in the experimental pattern, as a result of preferential orientation.

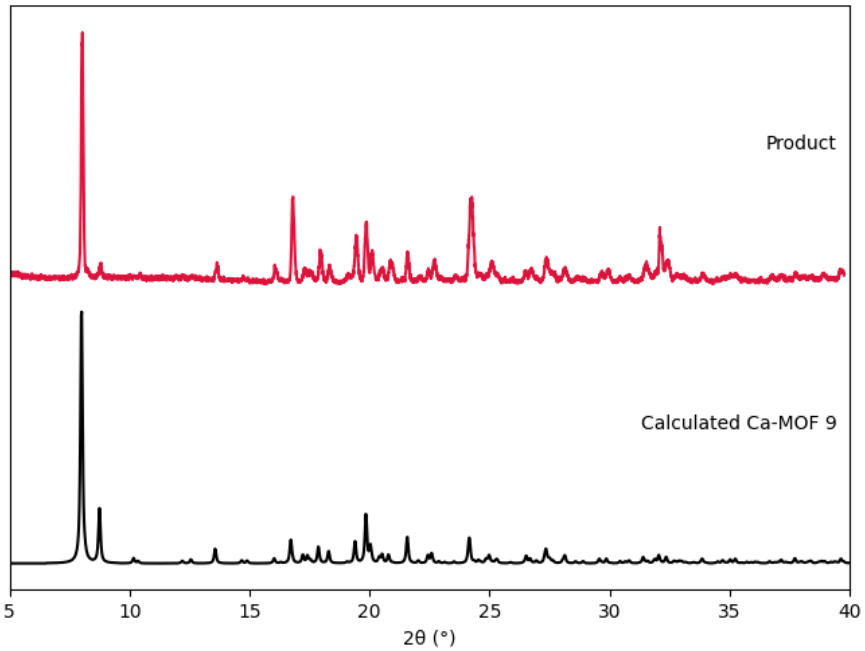

Fig. ESI8. Comparison of the PXRD diffractogram of a batch of Ca-MOF **9** (red, top) with the diagram calculated from single-crystal data (black, bottom).

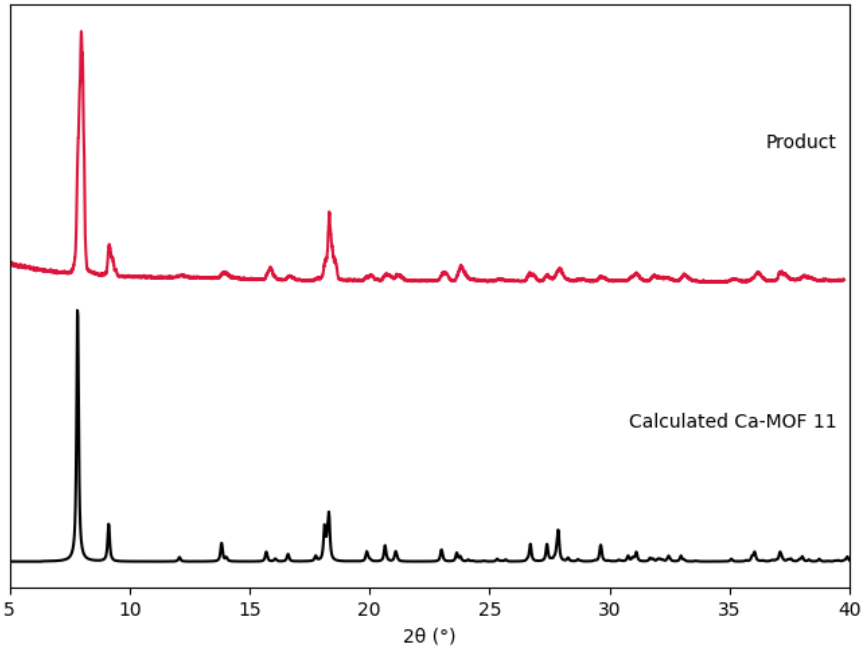

Fig. ESI9. Comparison of the PXRD diffractogram of a batch of Ca-MOF **11** (red, top) with the diagram calculated from single-crystal data (black, bottom).

Thermogravimetric analyses

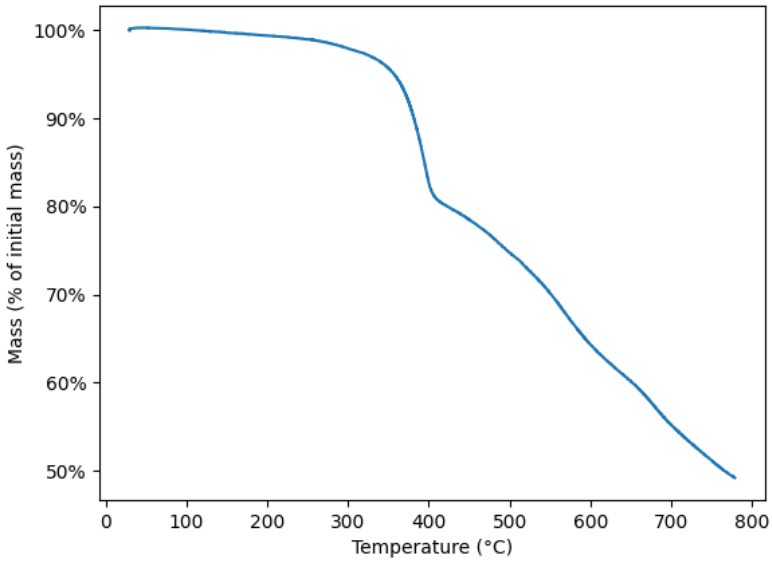

Fig. ESI10. TGA for Ca-MOF **2.**

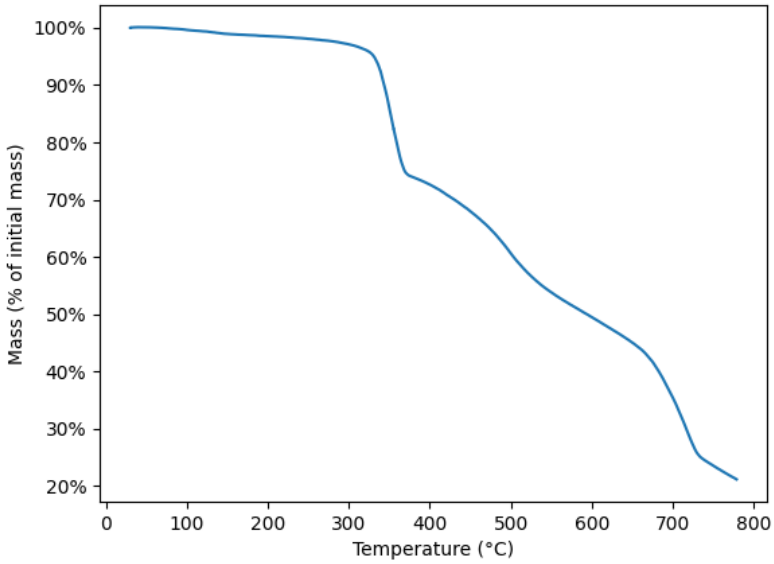

Fig. ESI11. TGA for Ca-MOF **3.**

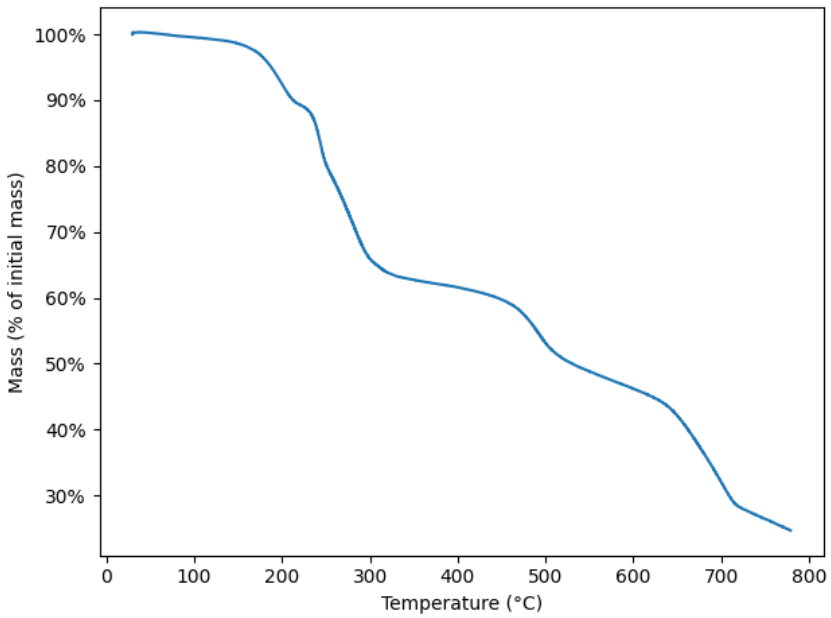

Fig. ESI12. TGA for Ca-MOF **4.**

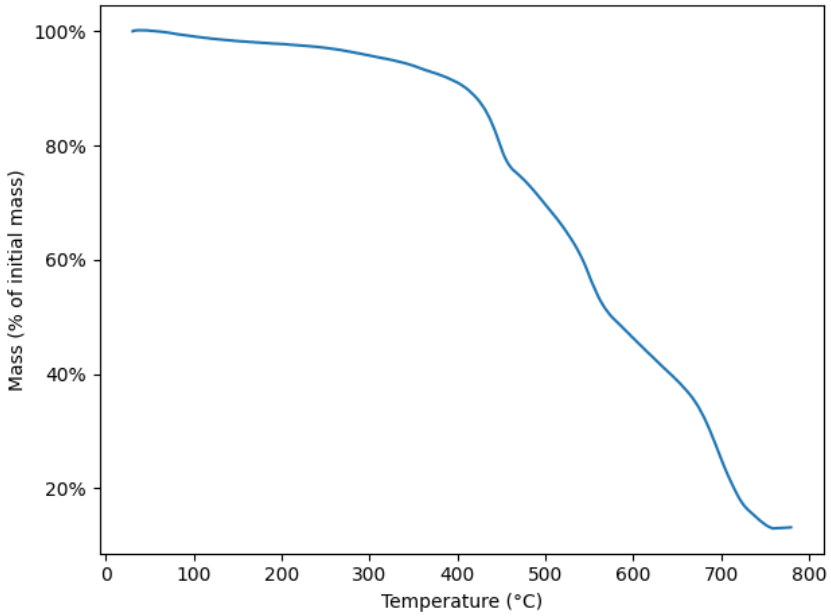

Fig. ESI13. TGA for Ca-MOF **7.**

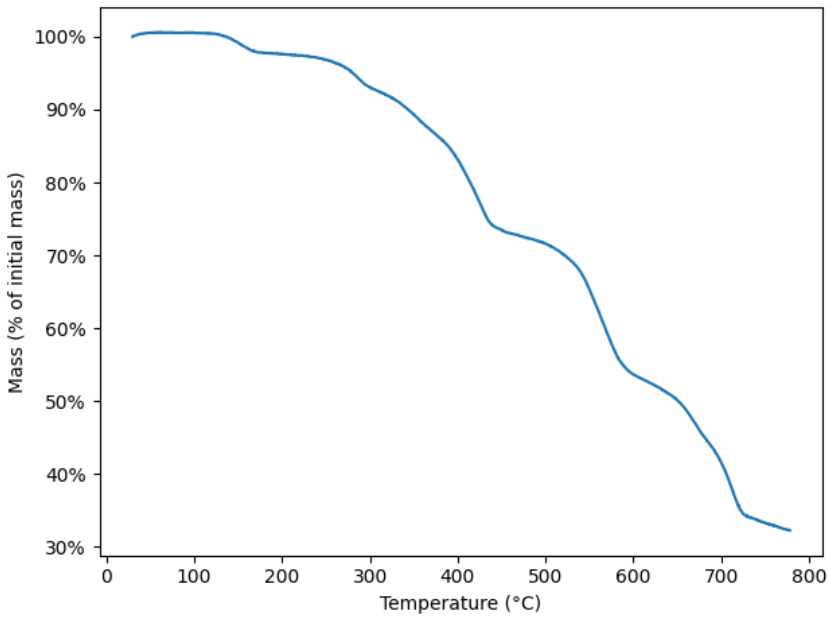

Fig. ESI14. TGA for Ca-MOF **8.**

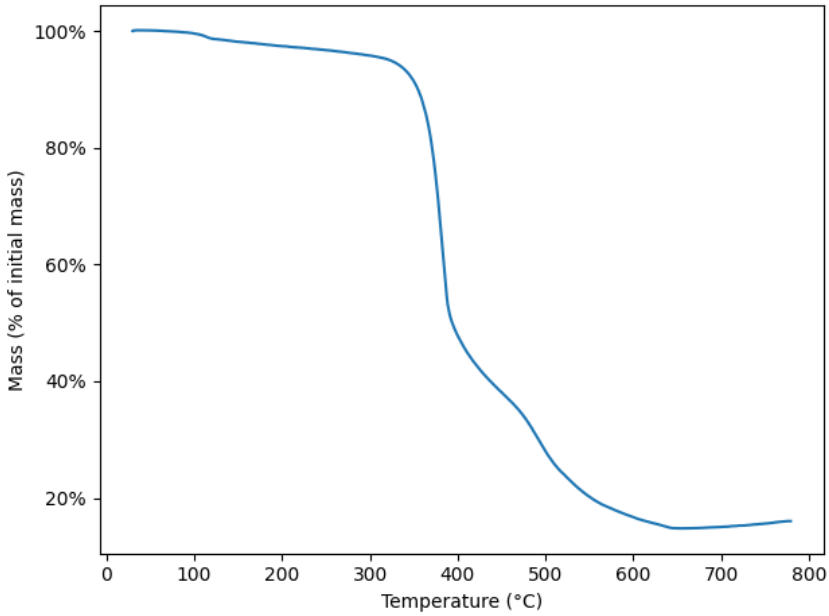

Fig. ESI15. TGA for Ca-MOF **9.**

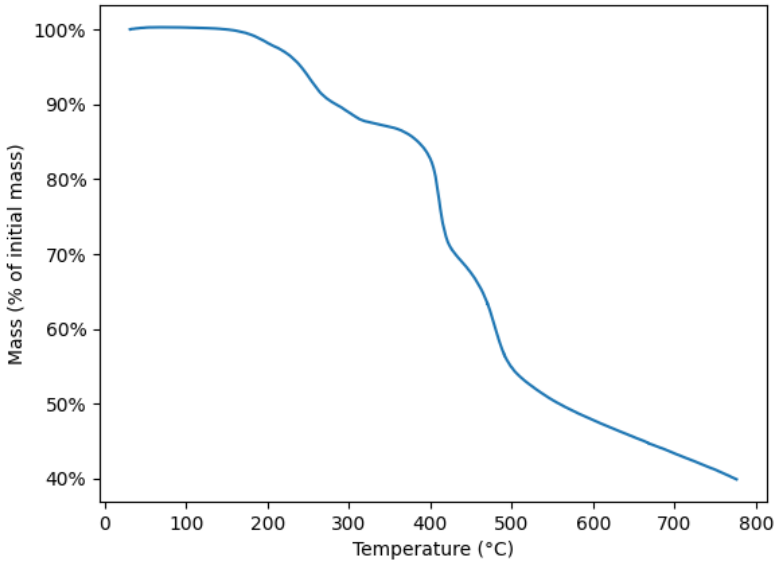

Fig. ESI16. TGA for Ca-MOF **10.**

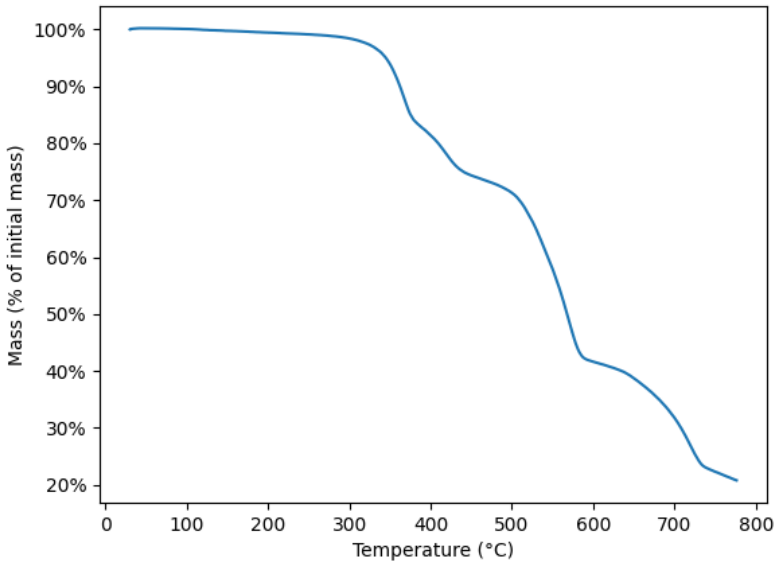

Fig. ESI17. TGA for Ca-MOF **11.**

Diffuse reflectance

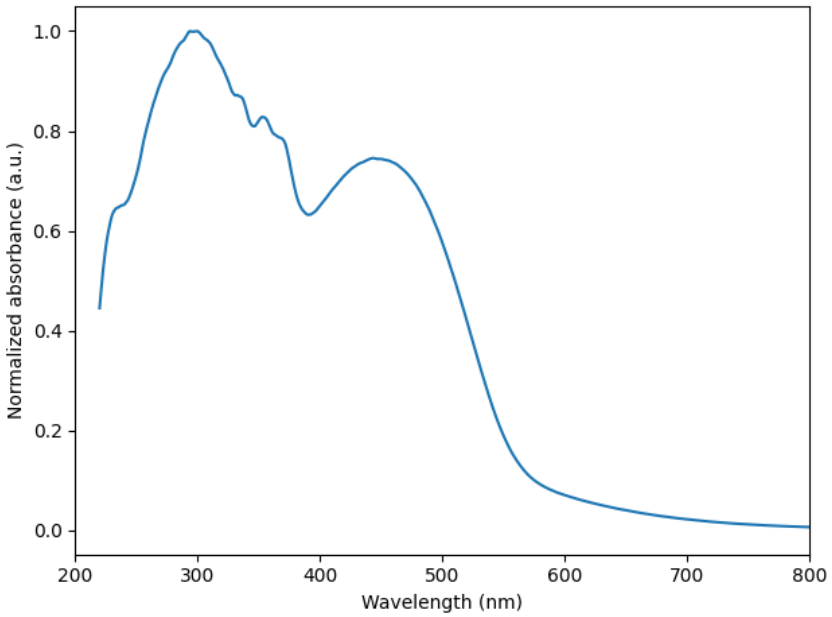

Fig. ESI18. Diffuse reflectance spectrum of Ca-MOF **2**.

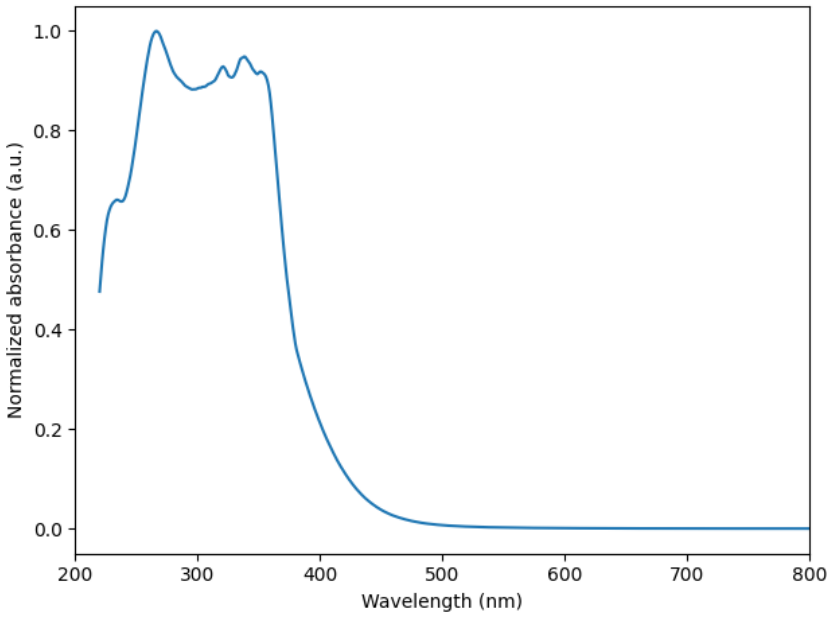

Fig. ESI19. Diffuse reflectance spectrum of Ca-MOF **3**.

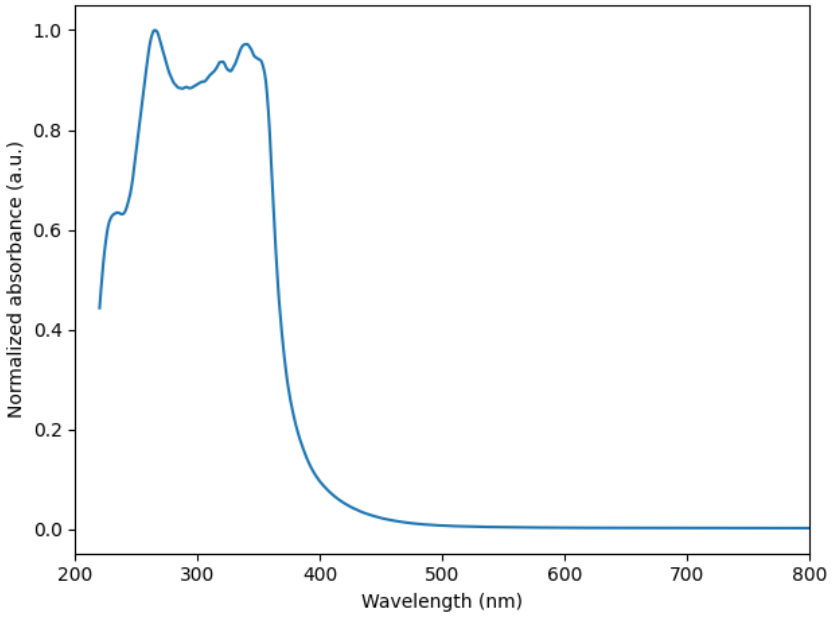

Fig. ESI20. Diffuse reflectance spectrum of Ca-MOF **4**.

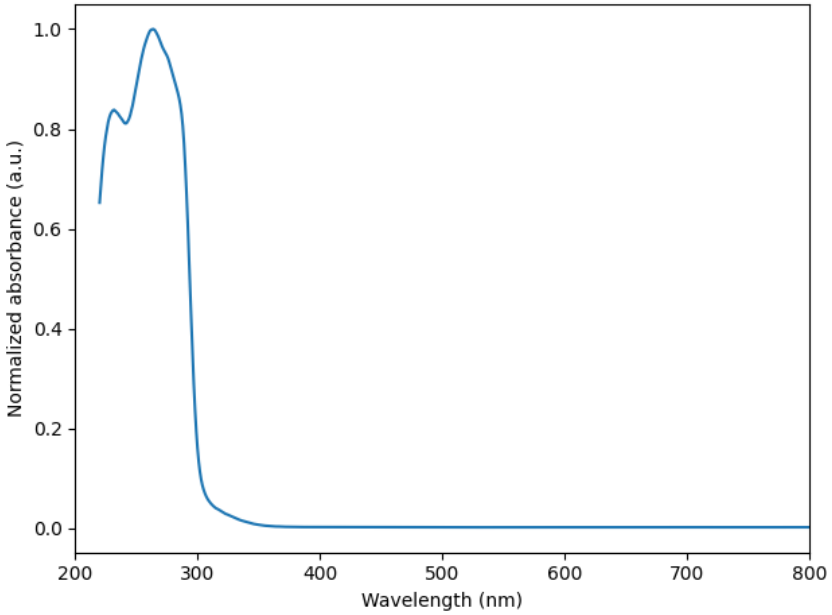

Fig. ESI21. Diffuse reflectance spectrum of Ca-MOF **7**.

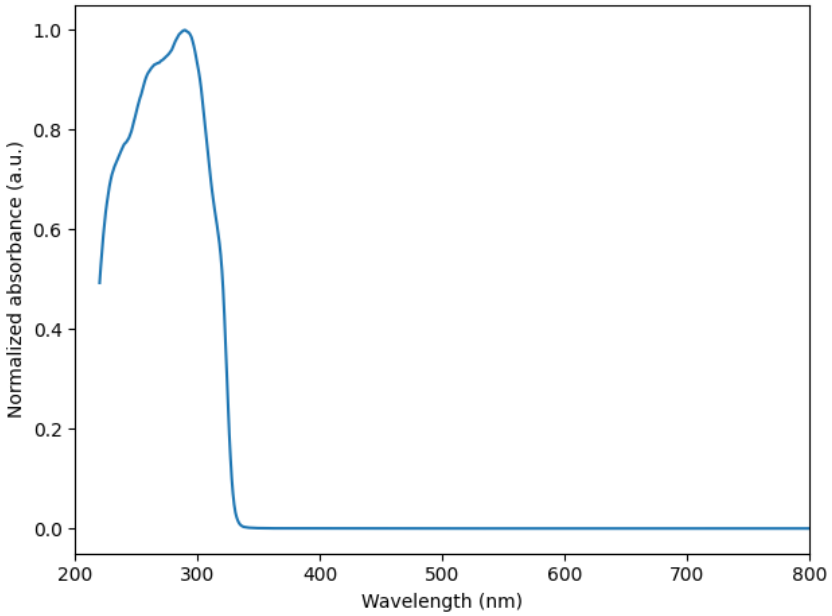

Fig. ESI22. Diffuse reflectance spectrum of Ca-MOF **8**.

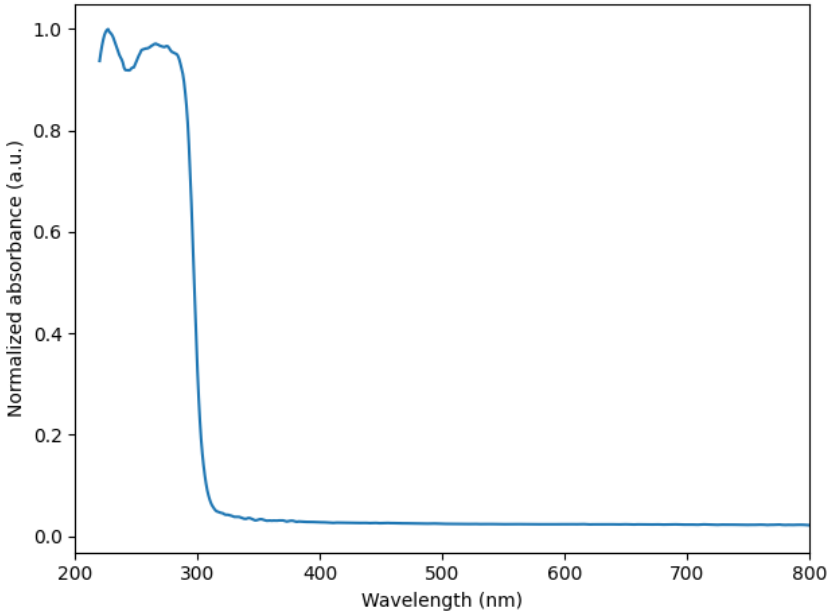

Fig. ESI23. Diffuse reflectance spectrum of Ca-MOF **9**.

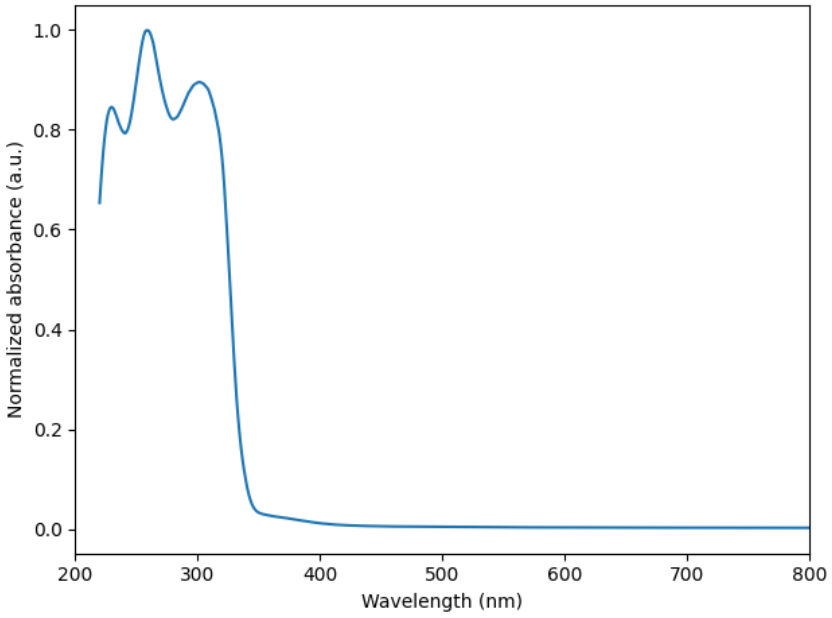

Fig. ESI24. Diffuse reflectance spectrum of Ca-MOF **10**.

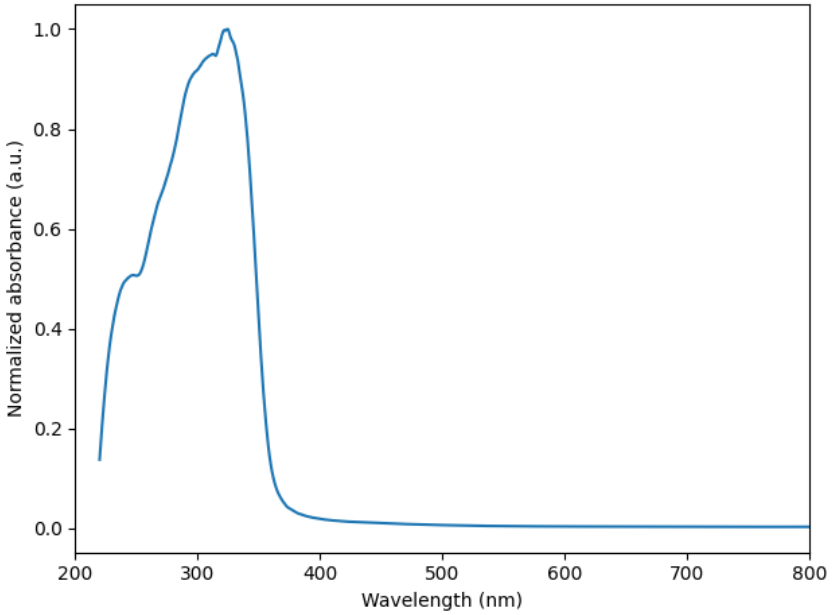

Fig. ESI25. Diffuse reflectance spectrum of Ca-MOF **11**.

Infra-red

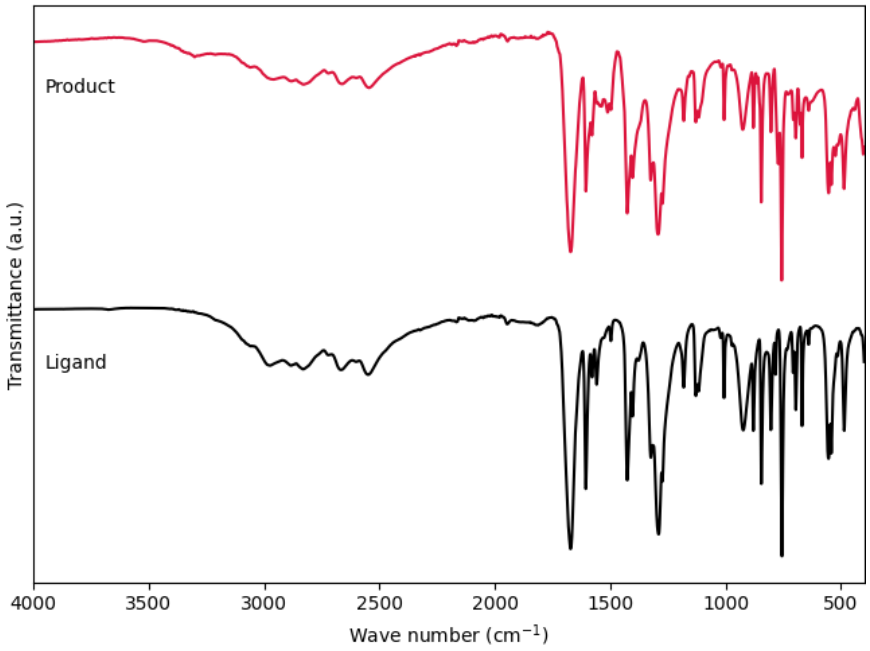

Fig. ESI26. Infra-red spectrum of Ca-MOF **1**.

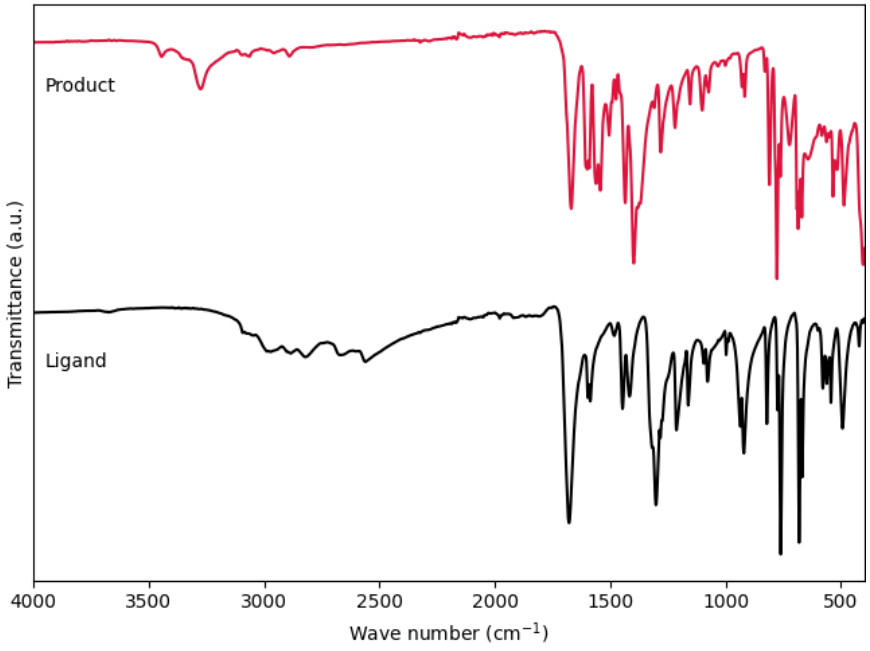

Fig. ESI27. Infra-red spectrum of Ca-MOF **2**.

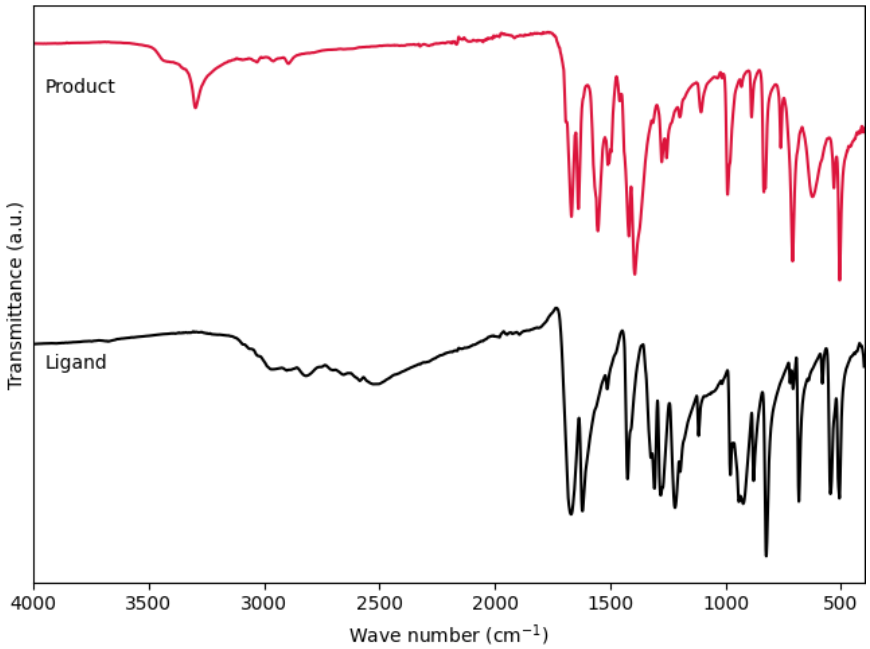

Fig. ESI28. Infra-red spectrum of Ca-MOF **3**.

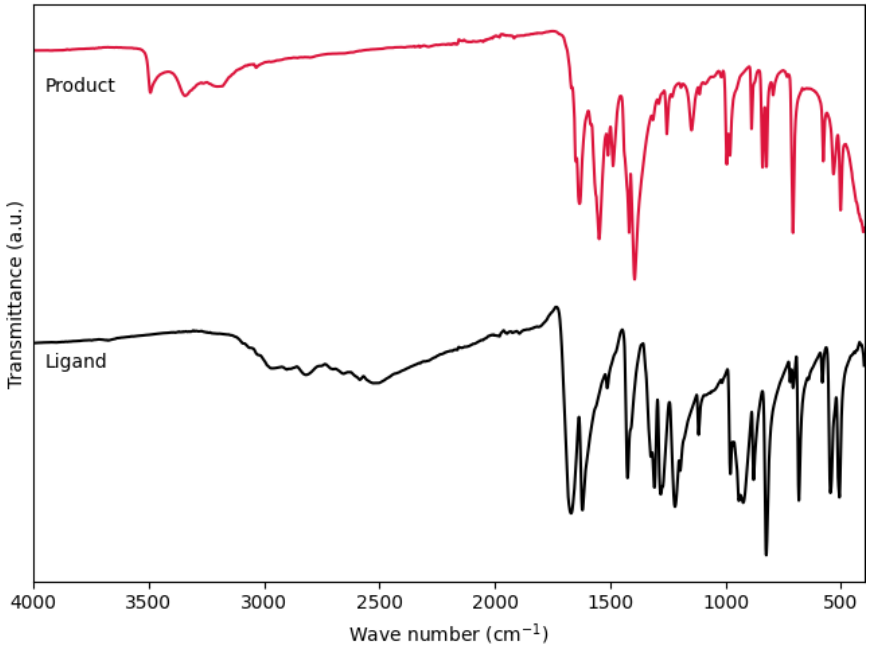

Fig. ESI29. Infra-red spectrum of Ca-MOF **4**.

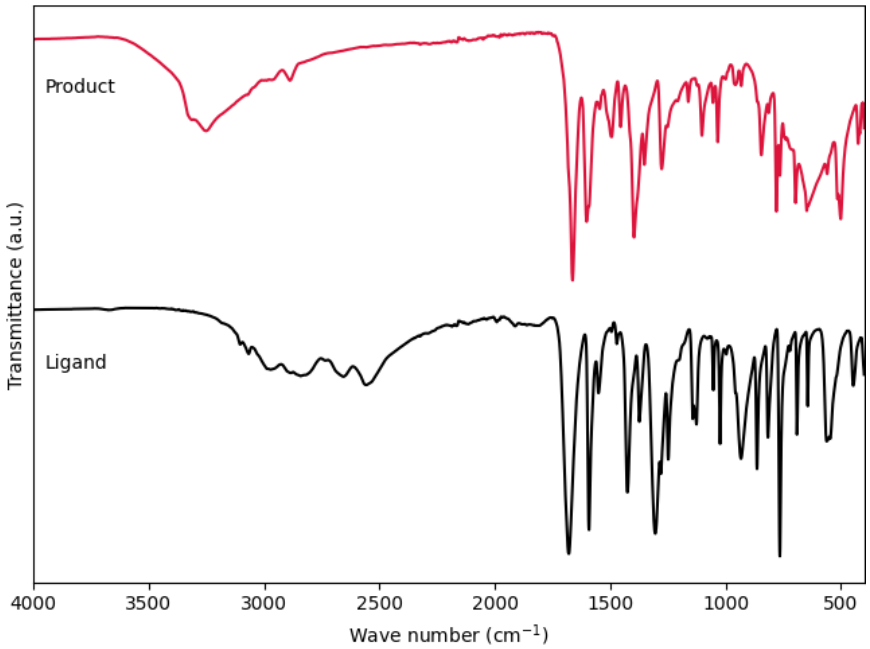

Fig. ESI30. Infra-red spectrum of Ca-MOF **5**.

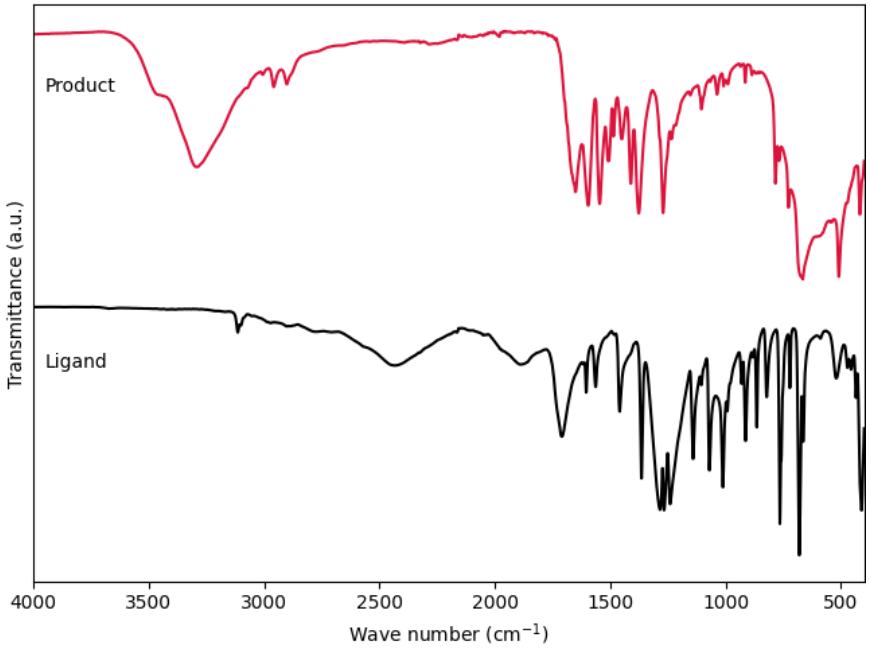

Fig. ESI31. Infra-red spectrum of Ca-MOF **6**.

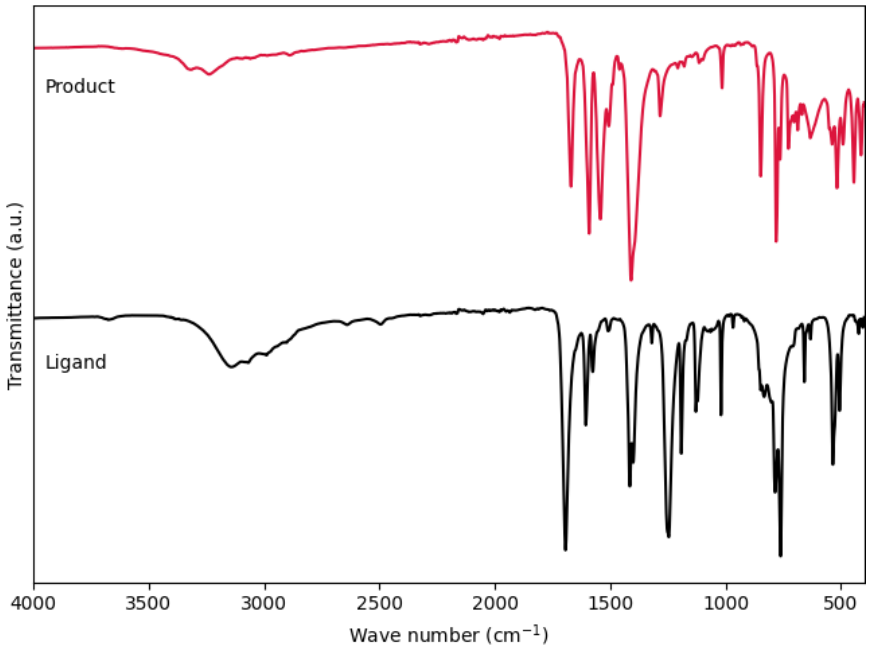

Fig. ESI32. Infra-red spectrum of Ca-MOF **7**.

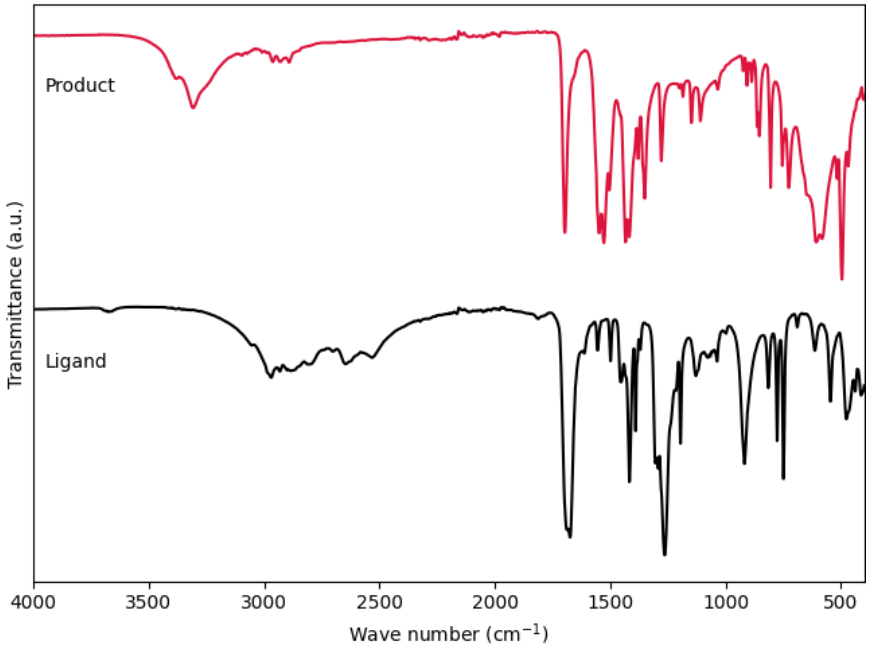

Fig. ESI33. Infra-red spectrum of Ca-MOF **8**.

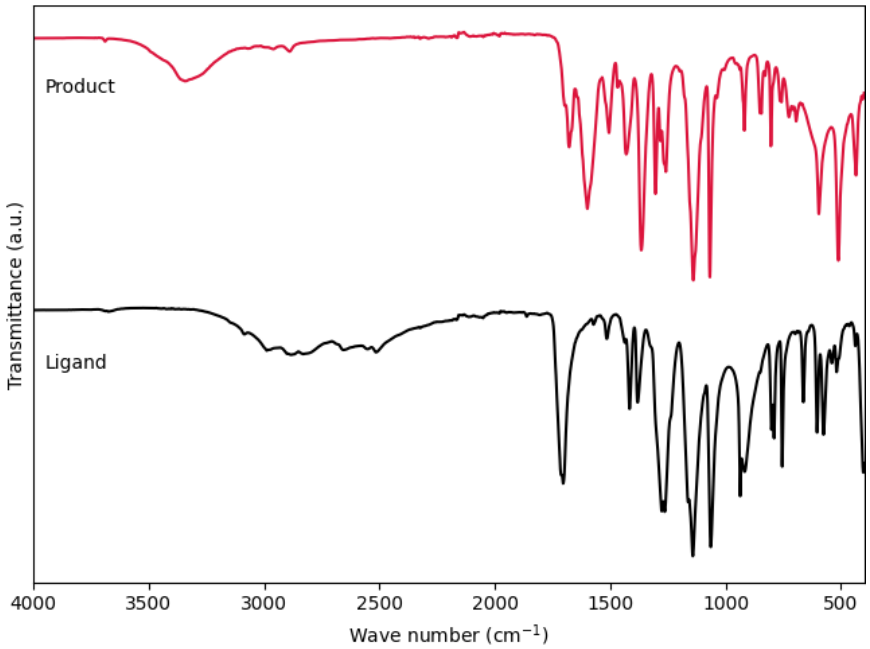

Fig. ESI34. Infra-red spectrum of Ca-MOF **9**.

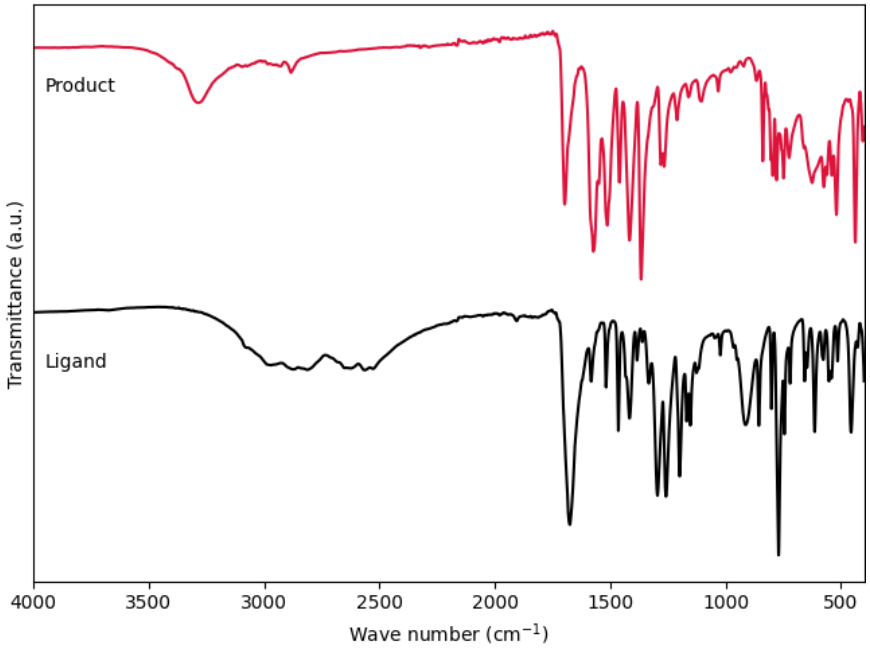

Fig. ESI35. Infra-red spectrum of Ca-MOF **11**.

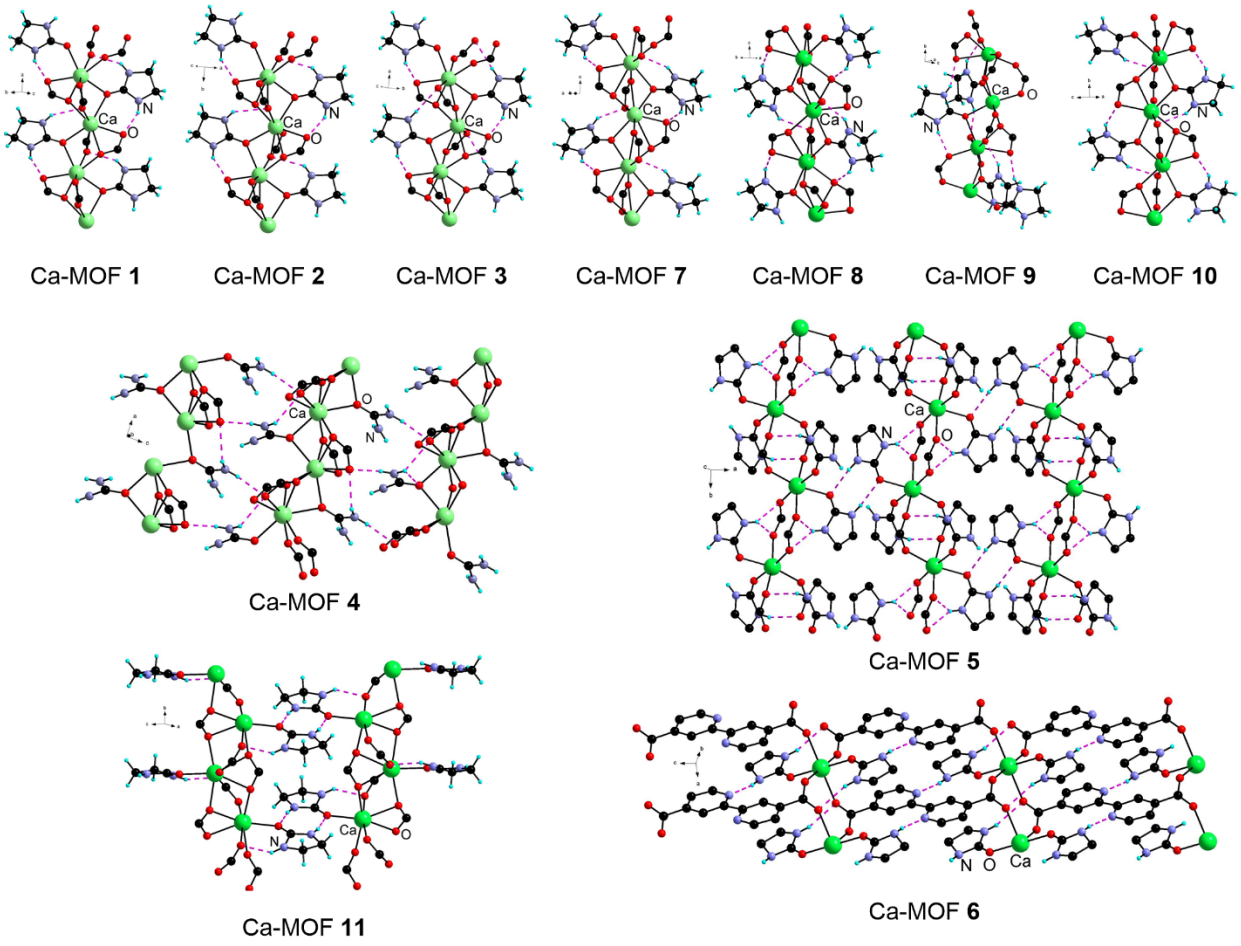

Fig. ESI36 Hydrogen bonding networks in Ca-MOFs **1**-**11**. Hydrogen bonds are presented as dotted purple lines.

Table ESI1. Distances and angles of hydrogen bonds involving the urea derivatives in Ca-MOFs **1**-**11**

Ca-MOF	$d_{N\text{-}H\bullet\bullet\bullet O}$ / Å	$\alpha_{N\text{-}H\bullet\bullet\bullet O}$ / °	$d_{N\text{-}H\bullet\bullet\bullet N}$ / Å	$\alpha_{N\text{-}H\bullet\bullet\bullet N}$ / °
1	2.757(5)	149.6		
	2.990(4)	142.2		
2	2.761(2)	147.5		
	3.151(2)	138.3		
3	2.761(4)	151.0		
	3.347(5)	177.8		
4	2.960(9)	116.9		
	2.968(5)	168.0		
5	2.992(4)	145.4		
	3.012(3)	133.4		
	3.099(4)	160.9		
6	3.042(3)	165.0	3.256(3)	172.0
7	2.821(6)	144.5		
8	2.750(2)	145.1		
	3.069(2)	139.3		
9	2.85(1)	149.2		
	2.89(1)	150.1		
	2.91(1)	147.6		
	2.95(1)	146.5		
10	2.789(6)	148.8		
	2.996(6)	148.4		
11	2.80(4)	139.0		
	2.909(7)	166.9		

Table ESI2. Experimental observation concerning attempted reactions in reline under conditions analogous to the ones employed in 1:2 ChCl:e-urea.

Ligand	Product	First few significant PXRD peaks
$pdaH_2$	Ca-MOF **4**	7.2°, 11.0°, 14.5°
$bpdcH_2$	Microcrystalline powder	6.4°, 10.9°, 12.9°
3,3'-azo-$bpdcH_2$	Microcrystalline powder	6.0°, 11.8°, 12.2°
5,5'-$bpydcH_2$	Microcrystalline powder	6.8°, 7.5°, 14.9°
4,4'-$bpydcH_2$	Microcrystalline powder	7.3°, 8.2°, 14.6°
Me_2bdcH_2	Microcrystalline powder	8.7°, 12.2°, 12.7°
Br_2bdcH_2	Microcrystalline powder	12.5°, 17.6°, 18.4°
$(CF_3)_2bdcH_2$	Microcrystalline powder	6.7°, 9.4°, 10.1°
1,4-$naphtH_2$	Microcrystalline powder	8.7°, 11.6°, 14.5°
$mtbH_4$	Microcrystalline powder	8.1°, 12.5°, 14.0°

Table ESI 3. Pore limiting and maximum pore diameters of 3D Ca-MOFs **1**-**4**, **7-11** determined using the pore analyzer module of the Mercury® software for the as-structurally determined material and for the materials where the coordinated urea derivatives have been removed (theoretically activated MOF with retention of the framework structure).

	As-structurally determined / Å		With urea derivatives theoretically removed/ Å	
Ca-MOF	Pore limiting ø	Maximum pore ø	Pore limiting ø	Maximum pore ø
1	1.69	2.39	3.92	4.26
2	1.26	2.05	4.00	4.43
3	1.56	2.54	3.89	4.16
4	1.34	2.18	2.18	3.08
7	1.79	2.53	3.78	4.36
8	0.94	1.87	3.34	4.45
9	1.98	3.00	4.03	5.37
10	1.48	4.19	3.79	5.20
11	0.92	1.84	2.89	4.36